Nonlinear Raman Probe of Single Molecules Attached to Colloidal Silver and Gold Clusters

Katrin Kneipp[1,2], Harald Kneipp[2], Irving Itzkan[1],
Ramachandra R. Dasari[1], Michael S. Feld[1], and Mildred S. Dresselhaus[1,3]

[1] Massachusetts Institute of Technology
Cambridge, MA 02139, USA
kneipp@usa.net
[2] Technical University Berlin
10623 Berlin, Germany
[3] Office of Science, Department of Energy
Washington DC 2058, USA

Abstract. We review surface-enhanced linear and nonlinear Raman scattering experiments on molecules and single wall carbon nanotubes attached to colloidal silver and gold clusters. Surface-enhanced hyper-Raman scattering and surface-enhanced anti-Stokes Raman scattering from pumped vibrational levels are studied as two-photon excited Raman processes where the scattering signal depends quadratically on the excitation laser intensity. The experimental results are discussed in the framework of strongly enhanced electromagnetic fields predicted for such cluster structures in so-called "hot spots." The electromagnetic enhancement factors for Stokes, pumped anti-Stokes, and hyper-Raman scattering scale as theoretically predicted, and the field strengths in the hot spots, it is inferred, are enhanced of the order of 10^3. From our experiments we claim a very small density of hot spots (0.01 % of the cluster surface) and lateral confinement of the strong field enhancement within domains that can be as small as 10 nm.

Effective cross sections of the order of 10^{-16} cm^2 and 10^{-42} cm^4 s for Stokes and pumped anti-Stokes scattering, respectively, are adequate for one- and two-photon Raman spectroscopy of single molecules.

1 Introduction

During the last decade, detecting and characterizing single molecules, including artificial large molecules, such as nanotubes or quantum dots, using laser spectroscopy became a matter of growing interest [1,2,3]. In general, since the spectroscopic signal is proportional to the number of molecules that contribute to the signal, single molecule spectroscopy means dealing with very low signals. Therefore, methods for enhancing optical signals are essential for developing single molecule spectroscopy. Exciting opportunities for enhancing spectroscopic signals exist, when the target species is attached to metallic nanostructures. In the very close vicinity of such structures, local optical fields can be strongly enhanced when they are in resonance with the collective excitation of conduction electrons, also called surface plasmon resonances. Particularly high field enhancement seems to exist for ensembles of

V. M. Shalaev (Ed.): Optical Properties of Nanostructured Random Media,
Topics Appl. Phys. **82**, 227–249 (2002)

metallic nanoparticles exhibiting fractal properties, such as colloidal silver or gold clusters formed by aggregation of colloidal particles or island films of those metals [4,5,6]. Plasmon resonances in such structures occur over a relatively wide distribution of frequencies and simultaneously, they tend to be spatially localized and enhanced in small areas, so-called "hot spots" whose dimensions can be smaller than tenths of a wavelength [7]. Very favorable conditions for single molecule spectroscopy exist when the target molecule is attached to a hot spot and can be probed by the high local optical fields. Moreover, the strong lateral confinement of the field enhancement provides an additional opportunity for selecting a single species. Hot areas on cluster structures provide particularly attractive opportunities for nonlinear probes of single molecules, where the signal depends on the enhanced field intensities raised to a power of two or greater.

Because of its high information content on chemical structure, Raman scattering is a very promising technique for single molecule spectroscopy. The information about a molecule is considerably increased when nonlinear Raman techniques are applied in addition to "normal" linear Raman scattering. For example, hyper-Raman scattering follows different selection rules than normal Raman scattering, and therefore it can probe so-called "silent modes" that are forbidden in normal Raman scattering and in infrared absorption [8,9]. The general disadvantage of Raman spectroscopy and also of nonlinear Raman spectroscopic techniques is the extremely small cross section that makes, for example, the use of hyper-Raman scattering nearly impossible as a practical "spectroscopic tool." Linear Raman scattering cross sections fall between $10^{-30}\,\mathrm{cm}^2$ and $10^{-25}\,\mathrm{cm}^2$ per molecule; the larger values occur under favorable resonance Raman conditions; hyper-Raman scattering has cross sections of approximately $10^{-65}\,\mathrm{cm}^4\,\mathrm{s}/$ photon.

In spite of these small cross sections, recently, single molecule Raman spectra have been measured by several groups (for an overview see [10]). The experiments are based on the phenomenon of a strongly increased Raman signal from molecules attached to metallic nanostructures, the effect of so-called "surface-enhanced Raman scattering" (SERS) [11,12,13]. The unexpectedly high Raman scattering signal from molecules attached to a metal substrate with nanometer-scaled structure or "roughness" [14,15,16] might be one of the most impressive effects for demonstrating the interesting optical properties of metallic nanostructures, which occur due to resonances with the plasmon excitations in the metal. In particular, strong enhancement has been observed when molecules are attached to colloidal silver or gold clusters or to island structures of those metals. The high local optical fields in the hot spots of such cluster structures provide a rationale for the high enhancement level, which is necessary for nonresonant single molecule Raman spectroscopy [17].

According to the electromagnetic field enhancement model, nonlinear Raman effects should be surface enhanced to a greater extent than "normal" Raman scattering. In agreement with this hypothesis, for molecules attached

to colloidal silver clusters, we obtained Raman scattering and hyper-Raman scattering at nearly the same signal level since the much stronger field enhancement for the nonlinear effect compensated for its smaller cross section [18,19].

In this article, we review surface-enhanced linear and nonlinear Raman scattering experiments. In particular, we want to discuss the feasibility of applying nonlinear Raman scattering to single molecules located in the hot areas of a metal cluster structure and the potential of SERS experiments performed on large artificial molecules such as single wall carbon nanotubes. Surface-enhanced hyper-Raman scattering and "pumped" anti-Stokes Raman scattering are selected as nonlinear or two-photon excited Raman probes where the Raman scattering signal depends quadratically on the excitation laser intensity. Our experimental findings in surface-enhanced Stokes, anti-Stokes, and hyper-Raman scattering as well as in surface-enhanced Raman scattering from single wall carbon nanotubes are discussed in the framework of a strong local electromagnetic field enhancement in the hot spots of colloidal metal clusters.

2 Surface-Enhanced Linear and Nonlinear Raman Scattering

In this section, we briefly introduce surface-enhanced linear and nonlinear Raman scattering and discuss experiments when the target species is attached to colloidal silver or gold clusters.

2.1 Experimental

Figure 1 shows the schematic of an experimental setup for surface-enhanced linear and nonlinear Raman spectroscopy on molecules attached to colloidal silver and gold clusters [20]. The colloidal cluster–target molecule complex is provided in aqueous solution or "dry" on a glass slide. Raman scattering is excited using an argon-ion laser pumped Ti:sapphire laser operating in the near infrared (NIR). The Raman light can be observed at the Stokes and anti-Stokes side of the NIR excitation laser. Hyper-Raman scattering can be measured at the Stokes side of the second harmonic of the NIR excitation laser in the near-ultraviolet region.

Surface-enhanced Stokes and anti-Stokes Raman spectra are excited in the CW mode of the Ti:sapphire laser using 10^4–$10^6\,\mathrm{W/cm^2}$ intensities. For surface-enhanced hyper-Raman studies, the laser is used in the mode-locked picosecond regime to achieve excitation intensities of about $10^7\,\mathrm{W/cm^2}$. Grating spectrographs were used to disperse the scattered light. Surface-enhanced Stokes and anti-Stokes Raman light (shifted relative to the NIR excitation) and surface-enhanced hyper-Raman light (shifted relative to the second harmonic of the NIR light) can be measured simultaneously in the

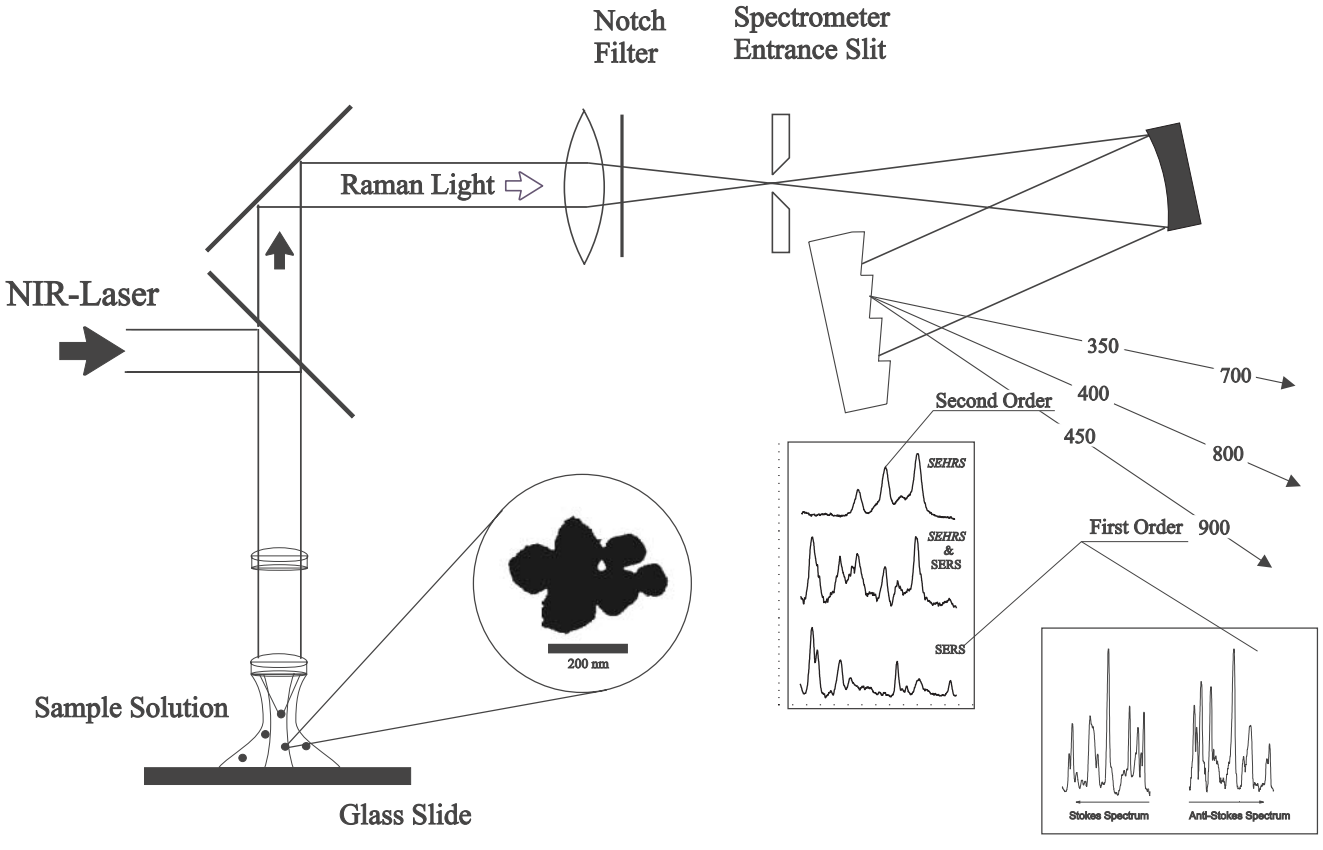

Fig. 1. Schematic experimental setup for surface-enhanced linear and nonlinear Raman spectroscopy

same spectrum using the first and second diffraction order of the spectrograph. This allows direct measurement of the ratio between SEHRS and SERS signal power [18,19]. The relative wavelength sensitivity of the system for Stokes Raman, compared to anti-Stokes Raman and hyper-Raman scattering, was determined by using Stokes and anti-Stokes Raman spectra of benzene measured at NIR excitation and its second harmonic.

2.2 Surface-Enhanced Linear Raman Scattering

Raman signals can be enhanced by more than 10 orders of magnitude, when the molecule is attached or in the very close vicinity of silver or gold structures in dimensions of tens of nanometers. In analogy to "normal" Raman scattering, the number of Stokes photons per second $P_{\mathrm{S}}^{\mathrm{SERS}}$ in surface-enhanced Raman scattering can be written as

$$P_{\mathrm{S}}^{\mathrm{SERS}} = N_0 \sigma_{\mathrm{s}}^{\mathrm{SERS}} n_{\mathrm{L}} \,, \tag{1}$$

where $\sigma_{\mathrm{S}}^{\mathrm{SERS}}$ describes an effective cross section of the surface-enhanced Raman process and S denotes the Stokes scattering. n_{L} is the photon flux density of the excitation laser which is equal to the incoming laser field $|E^{(0)}(\nu_{\mathrm{L}})|^2$ divided by $h\nu_{\mathrm{L}}$ and by the focus area. $E(\nu)$ is the field strength, and ν_{L} and ν_{S} are the laser and the Stokes frequencies with

$$\nu_{\mathrm{S}} = \nu_{\mathrm{L}} - \nu_{\mathrm{M}}$$

or

$$\nu_{\mathrm{aS}} = \nu_{\mathrm{L}} + \nu_{\mathrm{M}} \,. \tag{2}$$

ν_{M} is the molecular vibrational frequency and minus and plus stand for Stokes and anti-Stokes scattering, respectively. N_0 is the number of molecules in the vibrational ground state, that are involved in the SERS process.

It is generally agreed that more than one effect contributes to the enhancement of the Raman signal [11,12,13]. The enhancement mechanisms are roughly divided into so-called "electromagnetic" field enhancement effects and "chemical first layer" effects. The latter effects include enhancement mechanism(s) of the Raman signal, which can be explained in terms of specific interactions, i. e., electronic coupling between molecule and metal [21], resulting in a larger Raman cross section $\sigma_{\mathrm{ads}}^{\mathrm{RS}}$ compared to that of the molecule without coupling to the metal $\sigma_{\mathrm{free}}^{\mathrm{RS}}$. The electromagnetic field enhancement arises from an enhanced local optical field at the place of the molecule, described by field enhancement factors $A(\nu)$. Then, the SERS cross section can be written as

$$\sigma_{\mathrm{s}}^{\mathrm{SERS}} = \sigma_{\mathrm{ads}}^{\mathrm{RS}} |A(\nu_{\mathrm{L}})|^2 |A(\nu_{\mathrm{S}})|^2 \,, \tag{3}$$

where

$$|A(\nu)|^2 = \frac{|E(\nu)|^2}{|E^{(0)}(\nu)|^2} \,. \tag{4}$$

$E(\nu)$ are the local optical fields (laser and the scattered field) and $E^{(0)}(\nu)$ are the same fields in the absence of the metal nanostructures.

The SERS enhancement factor G_{SERS} for Stokes scattering is determined by the ratio of the effective SERS cross section $\sigma_{\mathrm{S}}^{\mathrm{SERS}}$ to the "normal" Raman cross section $\sigma_{\mathrm{S,free}}^{\mathrm{RS}}$,

$$G_{\mathrm{SERS}} = \frac{\sigma_{\mathrm{ads}}^{\mathrm{RS}}}{\sigma_{\mathrm{free}}^{\mathrm{RS}}} |A(\nu_{\mathrm{L}})|^2 |A(\nu_{\mathrm{S}})|^2 \,. \tag{5}$$

The first term in formula (5), $\sigma_{\mathrm{ads}}^{\mathrm{RS}}/\sigma_{\mathrm{free}}^{\mathrm{RS}}$, describes the "chemical" enhancement effect. Chemical SERS enhancement factors may contribute factors of 10 to 1000 to the total SERS enhancement [21,13]. The second term describes local-field enhancement effects.

The electromagnetic contribution to SERS enhancement strongly depends on the morphology of the metal nanostructures and on the dielectric constants of the metal (for an overview, see [11,12,13]). The field enhancement exhibits particularly exciting properties for fractal metallic nanostructures [22,5,6,4,23] and can reach 12 orders of magnitude for colloidal silver and gold cluster structures [24,25,26].

In the following, we discuss some experimental observations on SERS performed on colloidal silver and gold clusters. Figures 2a and 2b display Stokes and anti-Stokes SERS spectra of crystal violet attached to isolated colloidal gold spheres in aqueous solution. Figure 3a shows the electron micrographic view of one gold sphere and the extinction spectrum of the aqueous solution of many isolated spheres. NaCl was added to the aqueous solution to induce aggregation of the spheres, but spectra in Figs. 2a and 2b were measured in the first minutes after addition of the salt. No changes in the extinction spectrum of the colloidal solution were observed, indicating that no aggregation occurred during this time. Therefore, the electromagnetic SERS enhancement should be mainly related to isolated gold spheres of about 60 nm in diameter. On the other hand, if there is any additional "chemical" enhancement related to NaCl induced "active sites" [27], that effect should already exist. After several minutes, when changes in the extinction spectrum from curve *a* to curve *b* in Fig. 3 indicated the formation of colloidal gold clusters (see also electron micrographs in Fig. 3), the SERS Stokes signal strongly increased (Fig. 2c). Now a strong anti-Stokes spectrum also occurs, as shown in Fig. 2d. Particularly, higher frequency modes appear at unexpectedly high signal levels in the anti-Stokes spectrum. This behavior indicates a very high SERS enhancement since molecules that are "pumped" to the first excited vibrational levels due to the strong Raman process now contribute to the anti-Stokes signal in addition to the thermally excited molecules [24]. We discuss this "pumped" anti-Stokes Raman scattering as a nonlinear Raman process in more detail later. Here, we use the anti-Stokes scattering only for a rough estimate of the SERS enhancement factor. In the stationary case as in our CW experiments, SERS cross sections are inferred from anti-Stokes to

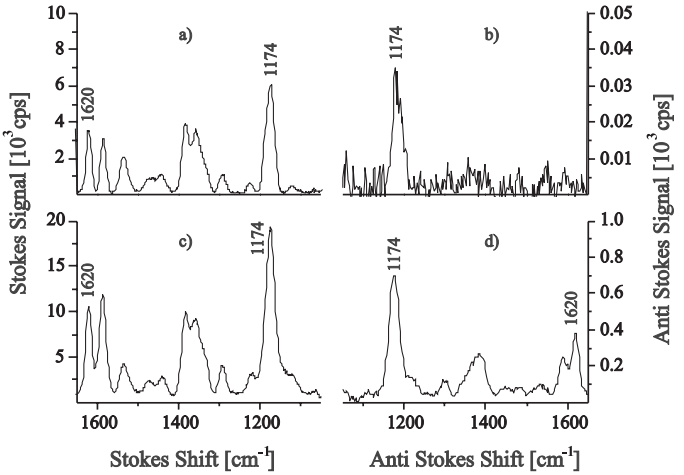

Fig. 2. Stokes (**a**, **c**) and anti-Stokes (**b**, **d**) SERS spectra of crystal violet on isolated colloidal gold spheres (**a**, **b**) and on colloidal gold clusters (**c**, **d**)

Stokes SERS signal ratios $P_{\mathrm{aS}}^{\mathrm{SERS}}/P_{\mathrm{S}}^{\mathrm{SERS}}$ normalized to the ratio in a normal Raman experiment $P_{\mathrm{aS}}^{\mathrm{RS}}/P_{\mathrm{S}}^{\mathrm{RS}}$ (Boltzmann population) according to [24]:

$$\frac{P_{\mathrm{aS}}^{\mathrm{SERS}}/P_{\mathrm{S}}^{\mathrm{SERS}}}{P_{\mathrm{aS}}^{\mathrm{RS}}/P_{\mathrm{aS}}^{\mathrm{RS}}} = \sigma^{\mathrm{SERS}}\tau_1 \mathrm{e}^{\frac{h\nu_{\mathrm{M}}}{kT}} n_{\mathrm{L}} + 1\,, \tag{6}$$

where τ_1 is the lifetime of the first excited vibrational state assumed to be of the order of 10 ps [28]. T is the sample temperature (300 K), and h and k are the Planck and Boltzmann constants, respectively [30].

In the anti-Stokes SERS spectrum measured from crystal violet on isolated gold spheres, the higher frequency anti-Stokes bands do not appear due to their weak thermal population. The anti-Stokes to Stokes signal ratio of the 1174 cm^{-1} crystal violet SERS line measured in Fig. 2a,b is in agreement with the ratio measured for the 1211 cm^{-1} line of toluene, which represents the Boltzmann population of the vibrational levels. That means that no Raman pumping can be observed for the smaller enhancement factors of isolated colloidal gold spheres since the effective Raman cross section is not large enough for measurably populating the first vibrational levels. According to formula (6), in SERS experiments on colloidal gold clusters, effective SERS cross sections on the order of $10^{-16}\,\mathrm{cm}^2$ per molecule must be operative, corresponding to total enhancement factors of about 10^{14} for a nonresonant Raman process in order to explain the observed anti-Stokes spectra.

Similar total enhancement factors of about 10^{14} were found for colloidal silver clusters. Figure 4 shows surface-enhanced Stokes and anti-Stokes Raman spectra of the DNA base adenine on colloidal silver clusters displaying the strong Raman line of the adenine ring breathing mode at 735 cm^{-1} and lines in the 1330 cm^{-1} region. As an indication of a very strong SERS effect,

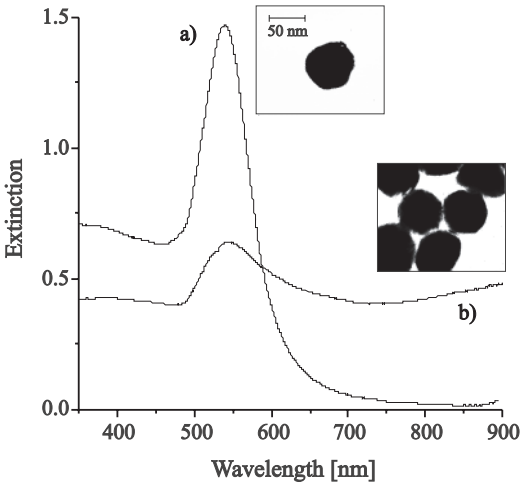

Fig. 3. Electron micrographs and extinction curves of isolated colloidal gold spheres and of colloidal clusters

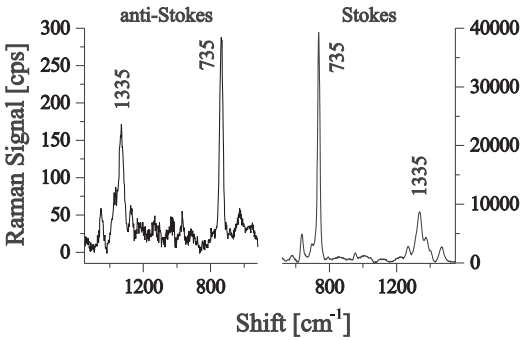

Fig. 4. NIR-SERS Stokes and anti-Stokes spectra of adenine measured on a silver cluster of about 8 µm. Parameters: 100 mW, 830 nm excitation with 1 µm spot size and 1 s collection time

higher frequency lines at the anti-Stokes side appear at relatively high signal levels, and effective Raman cross sections of the order of 10^{-16} cm^2/molecule can also be inferred for adenine [31]. Adenine has absorption bands in the ultraviolet. Therefore, at 830 nm excitation, no molecular resonance Raman effect will contribute to the large Raman cross section observed.

SERS enhancement factors of 10^{14}, as they are inferred from vibrational pumping, are also confirmed in single molecule Raman experiments. Figure 5a shows 100 Raman spectra measured in time sequence from a sample, which contains an average of 0.6 crystal violet molecules in the probed volume. Single target molecules are attached to colloidal silver clusters (see magnification glass in Fig. 1) and move into and out of the probed volume due to

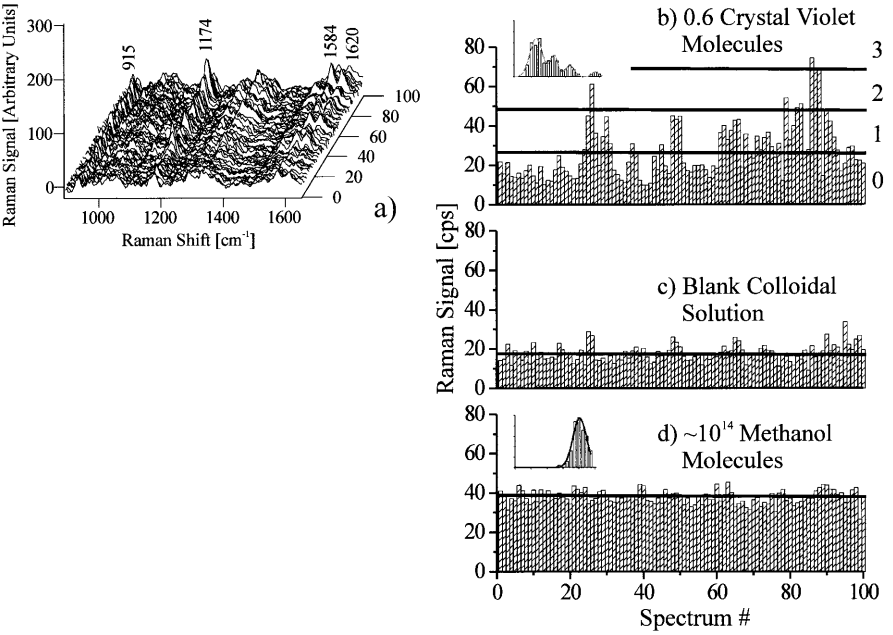

Fig. 5. Single molecule SERS spectra for confirming SERS enhancement factors of the order of 10^{14} (see text for explanation). (**a**) 100 SERS spectra collected from an average of 0.6 crystal violet molecules; (**b**) Peak heights of the 1174 cm^{-1} line; (**c**) background signal; (**d**) peak heights of a Raman line measured from $\sim 10^{14}$ methanol molecules. The *horizontal* lines display the thresholds for one-, two- and three-molecule signals (**b**), the average background (**c**), and the average 10^{14}-molecule signal (**d**). The *insets* in (**b**) and (**d**) show the Poisson and Gaussian statistics of single molecule and many molecule Raman signals, respectively. (Reprinted with permission from [25]. Copyright 1997 American Institute of Physics)

Brownian motion. Figure 5b displays the signal strengths of the 1174 cm^{-1} crystal violet peak in the 100 measurements showing a Poisson distribution for seeing just one, two, three, or, very likely zero molecules in the probed volume. Figure 5c shows the background signal at 1174 cm^{-1} when no crystal violet is in the sample. For comparison, Fig. 5d shows the signal of the 1030 cm^{-1} methanol Raman line, which comes from about 10^{14} methanol molecules in the probed volume. Methanol does not show SERS enhancement. A comparison between Figs. 5b and 5d shows that SERS signals of a single crystal violet molecule appear at the same level as the normal Raman signal of 10^{14} methanol molecules, confirming a SERS enhancement factor of the order of 10^{14} compared to a nonresonant Raman process [25].

2.3 Surface-Enhanced Raman Scattering from Single Wall Carbon Nanotubes

The theory predicts that extremely strong field enhancement is confined within very small areas, smaller than the wavelength of the light [7], but still large compared to the size of a molecule. Therefore, a single molecule SERS experiment performed on a "normal" molecule provides no information about the dimension of a hot spot. This can be different for large artificial molecules, such as single wall carbon nanotubes. A single wall carbon nanotube (SWNT) is a graphene sheet rolled up into a seamless cylinder to form a high aspect ratio (length/diameter) one-dimensional (1-D) macro-molecule, with a cylinder typically from 1 to 3 nm in diameter and a few microns long. SWNTs can be semiconducting or metallic, depending on the nanotube geometry. Raman spectroscopy provides a sensitive probe to distinguish semiconducting from metallic nanotubes through measurements on the tangential G-band feature near 1580 cm^{-1}. The variation in tube diameters results in small changes in the Raman frequencies for the tangential G band from tubes of different diameters [32]. Therefore, Raman spectra measured from a bundle of nanotubes, normally consisting of tubes with a diameter distribution, show inhomogeneously broadened Raman lines.

In our experiment, small bundles of single wall carbon nanotubes are attached to a fractal colloidal silver cluster [26]. When nanotubes are in contact with the cluster, the Raman signal can be enhanced by more than 10 orders of magnitude. Simultaneously, the inhomogeneous line width of the Raman line can strongly decrease. Figure 6 shows SERS spectra in the region of the tangential G band of semiconducting tubes measured from a bundle of tubes on a fractal silver cluster. The line width of the Raman band changes from place to place on the cluster, and in very rare cases, it becomes about 10 cm^{-1}. This value is very close to the theoretical homogeneous line width, suggesting that only a very small number of tubes, maybe even a single tube, just in contact with the cluster at a "hot spot," contributes to the SERS spectrum. Single wall carbon nanotubes have diameters between 1 and 3 nm; selecting a "few" tubes, or even a single tube, requires field confinement within less than 10 nm.

2.4 Pumped Anti-Stokes Raman Scattering

Anti-Stokes Raman scattering starts from the first excited vibrational levels and is proportional to the number of molecules in the first excited vibrational state N_1. This number N_1 relative to the number of molecules in the vibrational ground state N_0 is determined by the Boltzmann factor. As briefly discussed above, a strong surface-enhanced Raman Stokes process with an effective cross section $\sigma_{\mathrm{S}}^{\mathrm{SERS}}$ populates the first excited vibrational levels. Depopulation of these levels is determined by anti-Stokes scattering and by the vibrational lifetime τ_1. Figure 7 shows a schematic of

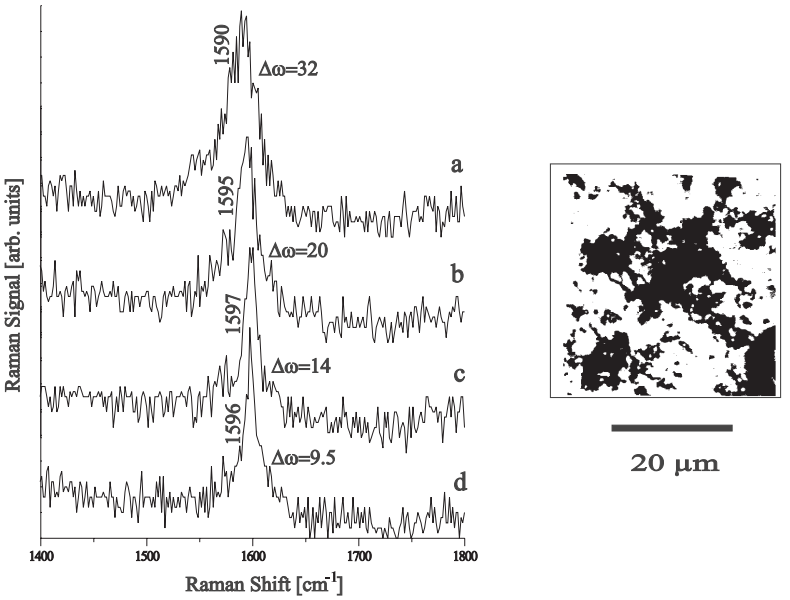

Fig. 6. SERS spectra of the tangential band of semiconducting single wall carbon nanotubes in contact with fractal colloidal silver clusters. Spectra measured with 1 μm spot size from different places on the cluster show different line widths of the Raman band (see text)

these processes and the appropriate rate equation for the number of molecules in the first excited vibrational state. In a weakly saturating intensity regime, $\exp(-h\nu_{\mathrm{M}}/kT) \leq \sigma_{\mathrm{S}}^{\mathrm{SERS}}\tau_1 n_{\mathrm{L}} \ll 1$ which in our experiments is between about $5\times10^5\,\mathrm{W/cm^2}$ and $1\times10^7\,\mathrm{W/cm^2}$, the anti-Stokes signal P_{aS} and the Stokes signal P_{S} can be estimated according to [24]

$$P_{\mathrm{aS}}^{\mathrm{SERS}} = (N_0 \mathrm{e}^{-\frac{h\nu_{\mathrm{M}}}{kT}} + N_0\sigma_{\mathrm{S}}^{\mathrm{SERS}}\tau_1 n_{\mathrm{L}})\sigma_{\mathrm{aS}}^{\mathrm{SERS}} n_{\mathrm{L}}\,, \tag{7}$$

$$P_{\mathrm{S}}^{\mathrm{SERS}} = N_0\sigma_{\mathrm{S}}^{\mathrm{SERS}} n_{\mathrm{L}}\,. \tag{8}$$

The second term in the equation for the anti-Stokes power $P_{\mathrm{aS}}^{\mathrm{SERS}}$ describes a quadratic dependence on the excitation intensity. This nonlinear anti-Stokes scattering

$$P_{\mathrm{aS,nl}}^{\mathrm{SERS}} = N_0\sigma_{\mathrm{aS,nl}}^{\mathrm{SERS}} n_{\mathrm{L}}^2 \tag{9}$$

can be described by an effective two-photon cross section

$$\sigma_{\mathrm{aS,nl}}^{\mathrm{SERS}} = \sigma_{\mathrm{S}}^{\mathrm{SERS}}\sigma_{\mathrm{aS}}^{\mathrm{SERS}}\tau_1\,. \tag{10}$$

Figure 8 shows plots of anti-Stokes and Stokes signal powers of crystal violet on colloidal gold clusters versus excitation laser intensities. The lines indicate

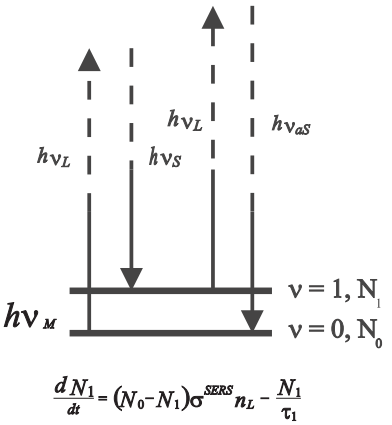

Fig. 7. Schematic Stokes and anti-Stokes Raman scattering

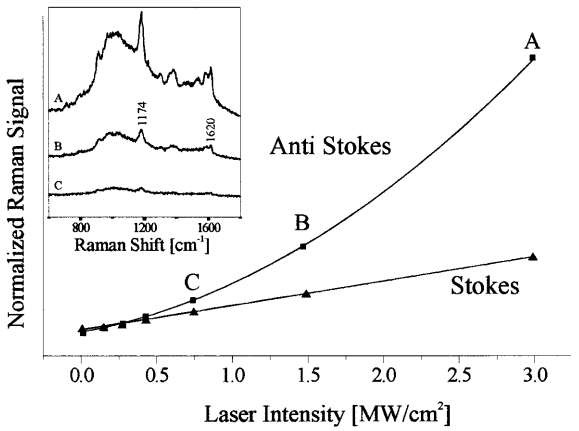

Fig. 8. Surface-enhanced Stokes (▲) and anti-Stokes (■) Raman scattering signals of the 1174 cm^{-1} line of crystal violet on colloidal gold clusters plotted vs 830 nm CW excitation intensity. The inset shows selected anti-Stokes spectra (A: 3 MW/ cm^2, B: 1.4 MW/ cm^2, and C: 0.7 MW/ cm^2). The Rayleigh background is suppressed by a notch filter up to about 900 cm^{-1}. (Reprinted with permission from [20]. Copyright 2000 SPIE)

quadratic and linear fits to the experimental data, displaying the predicted quadratic and linear dependence. The Stokes signal P_s^{SERS} always remains linearly dependent on the laser intensity. This behavior is different from nonlinear coherent anti-Stokes Raman scattering, which is generated by nonlinear coupling of the anti-Stokes and Stokes fields. In that case, the Stokes power also becomes nonlinearly dependent on the excitation laser intensity.

Assuming a SERS cross section of approximately $10^{-16}\,\mathrm{cm}^2$ and a vibrational lifetime of the order of 10 picoseconds, effective two-photon cross sections can be inferred at about $10^{-43}\,\mathrm{cm}^4\,\mathrm{s}$.

This provides a two-photon excited Raman probe at a cross section more than seven orders of magnitude larger than typical cross sections for two-photon excited fluorescence [33]. The large effective cross section can be explained by the nature of the process, which is a two-photon process exploiting the vibrational level as a real intermediate state.

Analogously to (3), we can split chemical and electromagnetic enhancement and write an expression for the effective surface-enhanced cross section for pumped anti-Stokes scattering:

$$\sigma_{\mathrm{aS,nl}}^{\mathrm{SERS}} = (\sigma_{\mathrm{ads}}^{\mathrm{RS}})^2 \tau_1 |A(\nu_{\mathrm{L}})|^4 |A(\nu_{\mathrm{S}})|^2 |A(\nu_{\mathrm{aS}})|^2 \,. \tag{11}$$

The enhancement factor of this nonlinear effect is [34]

$$G_{\mathrm{aS,nl}}^{\mathrm{SERS}} = \left(\frac{\sigma_{\mathrm{ads}}^{\mathrm{RS}}}{\sigma_{\mathrm{free}}^{\mathrm{RS}}} \right)^2 |A(\nu_{\mathrm{L}})|^4 |A(\nu_{\mathrm{S}})|^2 |A(\nu_{\mathrm{aS}})|^2 \,. \tag{12}$$

Because of its very high cross section, this two-photon effect can be observed at relatively low excitation intensities using CW lasers. For instance, at excitation photon flux densities of $10^{24}\,\mathrm{photons}/\,\mathrm{cm}^2\,\mathrm{s}$, the anti-Stokes signal appears at a signal level 20 times lower than the Stokes signal [35]. This confirms cross sections of the order of $10^{-42}\,\mathrm{cm}^4\,\mathrm{s}$ for the two-photon process.

Surface-enhanced pumped anti-Stokes Raman spectroscopy provides all the advantages of two-photon spectroscopy, such as a linear increase of the spectroscopic signal relative to the background for increasing excitation intensities. For illustration, the inset in Fig. 7 shows anti-Stokes spectra together with the Rayleigh background. Moreover, anti-Stokes spectra are measured at the high energy side of the excitation laser, which is free from fluorescence, since two-photon excited fluorescence appears at much higher frequencies. The two-photon process inherently confines the volume probed by surface-enhanced anti-Stokes Raman scattering compared to that probed by one-photon surface-enhanced Stokes scattering [20]. Similar effects of confinement of the probed volume are known from two-photon excited fluorescent detection of single molecules [36].

2.5 Surface-Enhanced Hyper-Raman Scattering (SEHRS)

Hyper-Raman scattering (HRS) is a spontaneous nonlinear process, i. e., different molecules independently scatter light due to their hyperpolarizability and generate an incoherent Raman signal shifted relative to the second harmonic of the excitation laser. The number of surface-enhanced hyper-Raman Stokes photons P^{SEHRS} can be written as

$$P^{\mathrm{SEHRS}} = N_0 \sigma^{\mathrm{SEHRS}} n_{\mathrm{L}}^2 \,, \tag{13}$$

where σ^{SEHRS} is the effective cross section for the surface-enhanced hyper-Raman process.

Hyper-Raman scattering can follow symmetry selection rules different from one-photon Raman scattering, and therefore HRS can probe vibrations that are forbidden in Raman scattering and also in infrared absorption [8,9]. The "normal" hyper-Raman cross section σ^{HRS} is extremely small, of the order of $10^{-65}\,\mathrm{cm}^4\,\mathrm{s}$. HRS can be enhanced analogously to normal Raman scattering by a "chemical" effect and by enhancement of the optical fields when the molecule is attached to metallic nanostructures. Then, the surface-enhanced hyper-Raman cross section is

$$\sigma^{\mathrm{SEHRS}} = \sigma^{\mathrm{HRS}}_{\mathrm{ads}} |A(\nu_{\mathrm{L}})|^4 |A(\nu_{\mathrm{HS}})|^2 \,, \tag{14}$$

where $\sigma^{\mathrm{HRS}}_{\mathrm{ads}}$ describes an enhanced hyper-Raman cross section compared to that of a "free" molecule [37]; the $A(\nu)$ describe the enhancement of the optical fields. We can write an enhancement factor for SEHRS as

$$G_{\mathrm{SEHRS}} = \frac{\sigma^{\mathrm{HRS}}_{\mathrm{ads}}}{\sigma^{\mathrm{HRS}}_{\mathrm{free}}} |A(\nu_{\mathrm{L}})|^4 |A(\nu_{\mathrm{HS}})|^2 \,. \tag{15}$$

Strong surface-enhancement factors can overcome the inherently weak nature of hyper-Raman scattering and surface-enhanced hyper-Raman spectra, and surface-enhanced Raman spectra can appear at comparable signal levels [18,19]. This is demonstrated in the middle spectrum in Fig. 9, which displays surface-enhanced hyper-Raman and Raman signals of crystal violet on colloidal silver clusters measured in the same spectrum (see also Fig. 1).

Taking into account the different sensitivity of the Raman system in the near-infrared and blue regions, the SEHRS signal is a factor of 100 weaker than the SERS signal. The experimental ratios between SERS and SEHRS intensities can be combined with the corresponding estimated "bulk" intensity ratio between RS and HRS scattering for the applied $10^7\,\mathrm{W/cm}^2$ excitation intensity (about 10^8 [9]) to infer a ratio of about 10^6 between surface-enhancement factors of hyper-Raman scattering and Raman scattering. Combining this ratio with NIR-SERS enhancement factors of crystal violet on colloidal silver clusters of the order of 10^{14}, total surface-enhancement factors of hyper-Raman scattering on crystal violet adsorbed on colloidal silver clusters of the order of 10^{20} can be inferred [38].

The enormous total enhancement factor for HRS, six orders of magnitude more than for "normal" RS, in principle, can be discussed in terms of a strong increase of the hyperpolarizibility due to interaction between the molecule and the metal electrons or by a strong field enhancement.

Figure 10 shows hyper-Raman spectra of crystal violet on colloidal silver clusters measured at different excitation wavelengths. The hyper-Raman signals decrease strongly with decreasing excitation wavelength. No hyper-Raman spectrum was measured at 760 nm excitation and below. This can be explained in the framework of a "field-enhancement model" where the

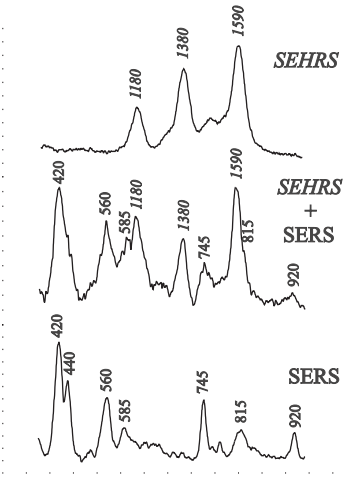

Fig. 9. SEHRS and SERS signals of crystal violet on colloidal silver clusters measured in the same spectrum using $10^7\,\mathrm{W/cm^2}$ NIR excitation (middle trace, see also Fig. 1). In the upper and the lower traces, SEHRS and SERS spectra are differentiated by placing a NIR absorbing filter in front of the spectrograph or by switching off the mode-locked regime of the Ti:sapphire laser, respectively

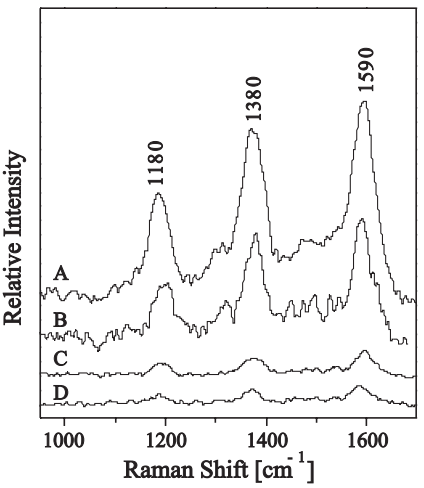

Fig. 10. Surface-enhanced hyper-Raman spectra of crystal violet on fractal colloidal silver clusters measured at 833 nm (A), 815 nm (B), 798 nm (C), and 785 nm (D). (Reprinted with permission from [38], Copyright 1999 Elsevier)

total enhancement benefits from enhancement of the laser and the scattering field (15). In general, field enhancement decreases for decreasing wavelengths. When the excitation wavelengths change from 830 to 750 nm, the wavelengths of the hyper-Raman fields change between 450 and 390 nm where field en-

hancement decreases rapidly [6]. At 750 nm excitation, the hyper-Raman Stokes field does not excite any eigenmodes on the colloidal silver cluster. This missing enhancement for the scattering field reduces the total enhancement to a level which is not sufficient to compensate for the extreme weakness of the hyper-Raman effect, and therefore we do not detect a hyper-Raman signal. This experimental finding supports the important role of electromagnetic enhancement in surface-enhanced hyper-Raman scattering.

The appearance of surface-enhanced hyper-Raman and Raman scattering at comparable scattering powers suggests that surface-enhanced hyper-Raman scattering is a spectroscopic technique that can be applied to single molecules.

3 Discussion

Extremely strong enhancement factors are observed for surface-enhanced linear and nonlinear Raman effects on colloidal silver and gold clusters at near-infrared excitation. Table 1 shows the effective cross sections observed in our experiments. For comparison, the table also shows typical cross sections for non-surface-enhanced optical processes.

The order of magnitude for the cross sections for "normal" linear SERS is confirmed in several experiments performed by other groups [39,40,41,42] (see Sect. 2.2), but most of these experiments, except [42], benefit from additional molecular resonance Raman enhancement.

In general, the strong enhancement of the Raman signal includes *electromagnetic* and *chemical* contributions. However, the experimental finding, that extremely large SERS enhancement is always related to colloidal silver or gold *clusters* [24,25,26,31,35,38,40,41,42,43,44] is an important indication that electromagnetic field enhancement plays a dominant role.

Figure 11 shows a typical fractal colloidal silver cluster structure used in our surface-enhanced linear and nonlinear NIR Raman experiments and the extinction spectrum of the aqueous solution of such clusters. The colloidal silver clusters have a fractal dimension of 1.63 ± 0.05 [45], in good agreement with values found for colloidal gold clusters [46]. Strongly enhanced

Table 1. Representative "normal" and surface-enhanced linear and nonlinear effective cross sections per molecule

Resonance Raman	10^{-16} cm^2
Fluorescence	10^{-16} cm^2
Two-photon fluorescence	10^{-50} cm^4 s/ photon
Hyper-Raman	10^{-65} cm^4 s/ photon
Pumped anti-Stokes Raman	10^{-71} cm^4 s/ photon
Surface-enhanced NIR-Raman	10^{-16} cm^2
Surface-enhanced pumped anti-Stokes Raman	10^{-43} cm^4 s/ photon
Surface-enhanced hyper-Raman	10^{-45} cm^4 s/ photon

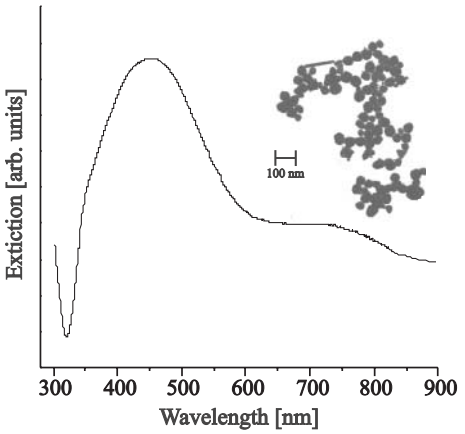

Fig. 11. Electron micrographs and extinction spectra of colloidal silver cluster structures used in the experiments

and highly localized fields, which are predicted for fractal colloidal cluster structures in so-called "hot spots" [5,6], can provide a rationale for the observed enhancement level. Moreover, plasmon resonances in a fractal cluster cover a broad frequency range from visible to the near infrared. This makes fractal clusters attractive for enhancing nonlinear effects, which very often involve optical fields at widely separated frequencies.

Note that for "normal" linear SERS, smaller clusters can show enhancement factors comparable to those obtained for fractal colloidal clusters. We also performed single molecule experiments on relatively small clusters 150–300 nm in size, formed by only 10–30 individual colloids (see for example [35]). Other authors have achieved single molecule sensitivity in SERS even for smaller clusters containing three to five colloidal particles [40,41,42]. Theoretical estimates for two particles in close contact show particularly strong electromagnetic enhancement at interparticle sites which result in electromagnetic SERS enhancement factors up to 10^{11} to 10^{12} [47], i. e., the same order of magnitude as SERS enhancement predicted for the hot spots on a fractal cluster [5,6]. But observation of surface-enhanced hyper-Raman scattering and strong vibrational pumping effects were possible only for cluster sizes of approximately 1 μ or larger. In particular, using small compact clusters, we did not observe surface-enhanced hyper-Raman scattering. This may be because the small compact clusters do not have such a broad plasmon resonance making it impossible that the laser and the hyper-Raman field can benefit simultaneously from plasmon resonance enhancement.

The surface of a fractal colloidal cluster structure shows a very inhomogeneous field distribution. This theoretical result was confirmed by near-field measurements [17]. SERS experiments performed on fractal cluster structures using relative high concentrations of the target molecule (about one mono-

layer on the fractal surface) also show that only a very small fraction (0.01 %) of the molecules available on the surface of the cluster can be involved in the Raman process at an extremely high enhancement level [24]. That means that total SERS enhancement factors of 14 orders of magnitude are available only at a few places on the cluster (about 0.01 % of the cluster surface).

SERS spectra performed on single wall carbon nanotubes show that the field enhancement on a fractal cluster is strongly confined within domains that can be as small as 10 nm.

Table 2 summarizes our experimental findings on the enhancement factors for nonresonant linear and nonlinear Raman scattering performed on fractal colloidal silver structures at near-infrared excitation. The first column shows the experimentally observed total enhancement factors [48].

We assume a "chemical" enhancement factor of about 100. This is the approximate order of magnitude we need to fill the gap between experimentally observed total SERS enhancement factors for small "NaCl activated" spheres [31] and electromagnetic estimates for such spheres [49]. The "chemical contribution" to the total enhancement should be preserved when colloidal particles form clusters.

Based on (5), (12), and (15), we can separate the "chemical" contribution to SERS enhancement. The third column in Table 2 then shows the value ascribed to electromagnetic enhancement. The table also shows the contributions to the electromagnetic enhancement factor from enhancing all optical fields involved in the process [50].

The estimate of the field-enhancement factors $A(\nu)$ for a fractal cluster is described in [6]. In general, these field-enhancement factors must be averaged over the cluster [6], but the numbers in the first column are experimental data taken from (single) molecules on "hot" spots, or the data are at least dominated by the Raman signals coming from these molecules [51]. Therefore, we believe that our experiments benefit from field-enhancement factors available in the hot spots of the cluster and do not represent average values.

In general, hot spots for different plasmon frequencies might be located at different places on the cluster, and the hot spot for a special Raman process is always a compromise. However, for small Raman shifts, both laser and scattered fields are very close, resulting in relative optimum field-enhancement conditions. Field enhancement for Stokes SERS and pumped anti-Stokes SERS should behave as a constant field-enhancement factor $A(\nu)$ raised to

Table 2. Enhancement factors of nonresonant linear and nonlinear Raman effects on fractal colloidal silver structures inferred from experiments using NIR excitation*

	Total	Field effect	
Raman scattering	10^{14}	10^{12}	$\lvert A(\nu_{\mathrm{L}})\rvert^2 * \lvert A(\nu_{\mathrm{S}})\rvert^2$
Hyper-Raman scattering	10^{20}	10^{18}	$\lvert A(\nu_{\mathrm{L}})\rvert^4 * \lvert A(\nu_{\mathrm{HRS}})\rvert^2$
Pumped anti-Stokes	10^{28}	10^{24}	$\lvert A(\nu_{\mathrm{L}})\rvert^4 * \lvert A(\nu_{\mathrm{aS}})\rvert^2 * \lvert A(\nu_{\mathrm{S}})\rvert^2$

* Assuming a factor of 10–100 "chemical" enhancement

the power of four and eight, respectively (see last column in Table 2). This agrees with our experimental results for a field-enhancement factor $A(\nu)$ of the order of 10^3. The experimentally observed enhancement factor for hyper-Raman scattering also scales quite well in this schema, at least for a long excitation wavelength (830 nm), where the hyper-Raman field is still in resonance with plasmon excitations of the silver cluster. This is surprising, since it is unlikely to find such an optimum spot for the large shift between the frequencies of laser field and hyper-Raman Stokes field, where all fields are enhanced by a factor 10^3 [52].

The importance of an enhancement of all fields is demonstrated by turning off the SEHRS effect when the frequency of the scattered field becomes too high to meet any plasmon resonance in the fractal (Fig. 10).

Effective cross sections of the order $10^{-16}\,\mathrm{cm}^2$ and $10^{-42}\,\mathrm{cm}^4\,\mathrm{s}$ for Stokes and pumped anti-Stokes scattering , respectively, allow one- and two-photon Raman spectroscopy of single molecules. Moreover, the different surface-enhanced linear and nonlinear Raman experiments on molecules and single wall carbon nanotubes on colloidal silver and gold clusters provide insight into the dimensions and the nature of the field enhancement of colloidal metal clusters.

References

1. M. J. Wirth, Chem. Rev. **99**, 2843 (1999) 227
2. X. S. Xie, J. K. Trautman, Annu. Rev. Phys. Chem. **49**, 441 (1998) 227
3. S. Nie, R. N. Zare, Annu. Rev. Biophys. Biomol. Struct. **26**, 567 (1997) 227
4. V. M. Shalaev, Phys. Rep. **272**, 61 (1996) 228, 232
5. V. M. Shalaev, Fractal Nano-Composites: Giant Local-Field Enhancement of Optical Responses, in: M. Bertolotti, C. M. Bowden, C. Sibilia (Ed.): *Nanoscale Linear and Nonlinear Optics* Proc. V. 560, (American Institute Physics, Melville, New York 2001) 228, 232, 243
6. V. M. Shalaev, *Nonlinear Optics in Random Media* (Springer, Berlin, Heidelberg 2000) 228, 232, 242, 243, 244
7. V. P. Safanov, V. M. Shalaev, V. A. Markel, Yu. E. Danilova, Ni. N. Lepeshkin, W. Kim, S. G. Raution, R. L. Armstrong, Phys. Rev. Lett. **80**, 1102 (1998) 228, 236
8. V. N. Denisov, B. N. Mavrin, V. B. Podobedov, Phys. Rep. **151**, 1 (1987) 228, 240
9. L. D. Ziegler, Raman Spectrosc. **21**, 769 (1990) 228, 240
10. K. Kneipp, H. Kneipp, I. Itzkan, R. R. Dasari, M. S. Feld, Chem. Rev. **99**, 2957 (1999) 228
11. A. Otto, Surface-enhanced Raman scattering: 'classical' and 'chemical' origins, in *Light Scattering in Solids IV. Electronic Scattering, Spin Effects, SERS and Morphic Effects*, M. Cardona, G. Güntherodt (Eds.) (Springer, Berlin, Heidelberg 1984) p. 289 228, 231, 232
12. M. Moskovits, Rev. Mod. Phys. **57**, 783 (1985) 228, 231, 232
13. A. Campion, P. Kambhampati, Chem. Soc. Rev. **27**, 241 (1998) 228, 231, 232

14. M. Fleischman, P. J. Hendra,, A. J. McQuillan, Chem. Phys. Lett. **26**, 123 (1974) 228
15. D. L. Jeanmaire, R. P. V. Duyne, J. Electroanal. Chem. **84**, 1 (1977) 228
16. M. G. Albrecht, J. A. Creighton, J. Am. Chem. Soc. **99**, 5215 (1977) 228
17. V. A. Markel, V. M. Shalaev, P. Zhang, W. Huynch, L. Tay, T. L. Haslett, M. Moskovits, Phys. Rev. B **59**, 10903 (1999) 228, 243
18. H. Kneipp, K. Kneipp, F. Seifert, Chem. Phys. Lett. **212**, 374 (1993) 229, 231, 240
19. K. Kneipp, H. Kneipp, F. Seifert, Chem. Phys. Lett. **233**, 519 (1995) 229, 231, 240
20. K. Kneipp, H. Kneipp, I. Itzkan, R. R. Dasari, M. S. Feld, Near-infrared surface-enhanced Raman spectroscopy of biomedically relevant single molecules on colloidal silver and gold clusters, SPIE Proc. **3922**, 49 (2000) 229, 238, 239
21. A. Otto, I. Mrozek, H. Grabhorn, W. Akeman, J. Phys. Cond. Matter **4**, 1143 (1992) 231, 232
22. M. I. Stockman, V. M. Shalaev, M. Moskovits, R. Botet, T. F. George, Phys. Rev. B **46**, 2821 (1992) 232
23. E. Y. Poliakov, V. M. Shalaev, V. A. Markel, R. Botet, Opt. Lett. **21**, 1628 (1996) 232
24. K. Kneipp, Yang Wang, H. Kneipp, I. Itzkan, R. R. Dasari, M. S. Feld, Phys. Rev. Lett. **76**, 2444 (1996) 232, 233, 237, 242, 244
25. K. Kneipp, Yang Wang, H. Kneipp, L. T. Perelman, I, Itzkan, R. R. Dasari, M. S. Feld, Phys. Rev. Lett. **78**, 1667 (1997) 232, 235, 242, 247
26. K. Kneipp, H. Kneipp, P. Corio, S. D. M. Brown, K. Shafer, J. Motz, L. T. Perelman, E. B. Hanlon, A. Marulci, G. Dresselhaus, M. S. Dresselhaus, Phys. Rev. Lett. **84**, 3470 (2000) 232, 236, 242
27. P. Hildebrandt, M. Stockburger, J. Phys. Chem. **88**, 5935 (1984) 232
28. W. Kaiser, J. P. Maier, A. Selmeier, in *Laser Spectroscopy IV*, H. Walther, E. Rothe (Eds.) (Springer, Berlin, Heidelberg 1979) 233
29. T. L. Haslett, L. Tay, M. Moskovits, Chem. Phys. **113**, 1641 (2000) 246
30. Deviations of the anti-Stokes to Stokes signal ratios from those expected from a Boltzmann population can also be observed when the resonance Raman conditions for anti-Stokes and Stokes scattering are different. Since the resonance Raman effect depends on resonance conditions of both excitation laser and the scattered light, the anti-Stokes scattering may benefit in some special circumstances from some preresonance Raman effect. This can occur, in particular, at excitation wavelengths in the NIR for molecules with absorption bands in the visible. In that case, the anti-Stokes to Stokes signal ratio also shows deviations from the Boltzmann ratio [29]. But this effect is independent of the excitation laser intensity. An indication for vibrational pumping is also a linear increase of the anti-Stokes to Stokes signal ratio or a quadratic dependence of the anti-Stokes signal power vs. the excitation laser intensity (see Sect. 2.4). 233
31. K. Kneipp, H. Kneipp, V. B. Kartha, R. Manoharan, G. Deinum, I. Itzkan, R. R. Dasari, M. S. Feld, Phys. Rev. E **57**, R6281 (1998) 234, 242, 244, 247
32. M. S. Dresselhaus, P. Eklund, Adv. Phys. **49**, 705 (2000) 236
33. J. Mertz, C. Xu, W. W. Web, J. Opt. Soc. Am. B **13**, 481 (1996) 239
34. The enhancement factor is determined relative to a fictive process, the population of excited vibrational states by spontaneous Raman scattering. For a

typical nonresonant Raman cross section of 10^{-30} cm^2 and vibrational lifetimes of about 10 ps, laser intensities on the order of 10^{20} W/cm^2 would be required to generate a measurable vibrational population 239
35. K. Kneipp, H. Kneipp, G. Deinum, I. Itzkan, R. R. Dasari, M. S. Feld, Appl. Spectrosc. **52**, 175 (1998) 239, 242, 243
36. J. Mertz, C. Xu, W. W. Webb, Opt. Lett. **20**, 2532 (1995) 239
37. J. T. Golab, J. R. Sprague, K. T. Carron, G. C. Schatz, R. P. van Duyne, J. Chem. Phys. **88**, 7942 (1988) 240, 247
38. K. Kneipp, H. Kneipp, I. Itzkan, R. R. Dasari, M. S. Feld, Chem. Phys. **247**, 155 (1999) 240, 241, 242
39. S. Nie, S. R. Emory, Science **275**, 1102 (1997) 242
40. H. Xu, E. J. Bjerneld, M. Kåll, L. Borjesson, Phys. Rev. Lett. **83**, 4357 (1999) 242, 243
41. M. Michaels, M. Nirmal,, L. E. Brus, J. Am. Chem. Soc. **121**, 9932 (1999) 242, 243
42. E. Bjernheld, P. Johansson,, M. Kaell, private communication (2000) 242, 243
43. K. Kneipp, Exp. Technik Phys. **36**, 161 (1988) 242
44. K. Kneipp, Y. Wang, R. R. Dasari, M. S. Feld, Appl. Spectrosc. **49**, 780 (1995) 242
45. K. Güldner, R. Liedtke, K. Kneipp, H. J. Eichler, Morphological Study of Colloidal Silver Clusters Employed in Surface-Enhanced Raman Spectroscopy (SERS), Europhys. Conf. Abstr., H. D. Kronfeldt (Ed.) (European Physical Society, Berlin 1997) Vol. 21 C, p. 128 242
46. D. A. Weitz, M. Oliveria, Phys. Rev. Lett. **52**, 1433 (1984) 242
47. H. Xu, J. Aizpurua, M. Kaell, P. Apell, Phys. Rev. E **62**, 4318 (2000) 243
48. It is worth noting that the total enhancement factor for normal Raman scattering was derived from vibrational pumping and independently, from a very straightforward experiment by comparing the nonenhanced Raman signal from 10^{14} methanol molecules and the surface-enhanced Raman signal from one molecule attached to a colloidal silver cluster. Also the ratio between SEHRS and SERS signals is measured in a manner in which experimental errors can be excluded (see Sect. 2.5) 244
49. D. S. Wang, M. Kerker, Phys. Rev. B **24**, 1777 (1981) 244
50. K. Kneippy, Exp. Technik Phys. **38**, 3 (1990) 244
51. In single molecule experiments, we detected between 70 and 80 % of the molecules [25,31]. This implies that it is very likely that molecules attach to the cluster just at the "hot" spots 244
52. There is also a possibility that hyper-Raman scattering benefits from a larger "chemical" enhancement effect than Raman scattering, which may compensate for the more unfavorable conditions for field enhancement [37] 245

Index